



Increasing the sensitivity of terahertz split ring resonator metamaterials for dielectric sensing by localized substrate etching

K. MENG,¹ S. J. PARK,^{1,*} A. D. BURNETT,² T. GILL,¹ C. D. WOOD,¹ M. ROSAMOND,¹ L. H. LI,¹  L. CHEN,¹ D. R. BACON,¹ J. R. FREEMAN,¹  P. DEAN,¹  Y. H. AHN,³  E. H. LINFIELD,¹  A. G. DAVIES,¹  AND J. E. CUNNINGHAM¹ 

¹*School of Electronic and Electrical Engineering, University of Leeds, Woodhouse Lane, Leeds, LS2 9JT, United Kingdom*

²*School of Chemistry, University of Leeds, Woodhouse Lane, Leeds, LS2 9JT, United Kingdom*

³*Department of Physics and Department of Energy Systems Research, Ajou University, Suwon 16499, South Korea*

**s.park@leeds.ac.uk*

Abstract: We demonstrate a significant enhancement in the sensitivity of split ring resonator terahertz metamaterial dielectric sensors by the introduction of etched trenches into their inductive-capacitive gap area, both through finite element simulations and in experiments performed using terahertz time-domain spectroscopy. The enhanced sensitivity is demonstrated by observation of an increased frequency shift in response to overlaid dielectric material of thicknesses up to 18 μm deposited on to the sensor surface. We show that sensitivity to the dielectric is enhanced by a factor of up to ~ 2.7 times by the incorporation of locally etched trenches with a depth of ~ 3.4 μm , for example, and discuss the effect of the etching on the electrical properties of the sensors. Our experimental findings are in good agreement with simulations of the sensors obtained using finite element methods.

Published by The Optical Society under the terms of the [Creative Commons Attribution 4.0 License](https://creativecommons.org/licenses/by/4.0/). Further distribution of this work must maintain attribution to the author(s) and the published article's title, journal citation, and DOI.

1. Introduction

In general, metamaterial sensors are designed to resonate strongly with electromagnetic waves at a specific frequency, determined by geometrical factors such as gap width, metal thickness, and the periodicity of the elements in the array from which they are formed [1–6]. Various resonances in metamaterials such as the inductive-capacitive (*LC*) resonance [7,8], dipole resonance [9], and quadrupole resonance [10] can be employed, whereby surface current modes are strongly excited by interaction with the incident electromagnetic radiation. The frequency of the *LC* resonance in split-ring resonators (SRRs), which have received particular attention [11–13], can be described by $1/2\pi\sqrt{LC}$, where *C* is the capacitance of the gap and *L* is the inductance of the ring [14,15]. This *LC* resonance in SRRs is particularly attractive in the context of sensing applications since the presence of dielectric materials in the gap area directly induces a frequency shift [16–19]. The effect of various geometrical parameters, including gap width, metal thickness, and substrate index on dielectric sensing using terahertz (THz) metamaterials have been explored in some detail [20–22]. Recent examples of sensing using SRR arrays include the detection of low-density nano / microscale microorganisms [1,18,23]. A noteworthy enhancement of the sensitivity was recently obtained by both by substituting for lower-index materials (e.g. quartz) for the higher-index substrate materials usually employed (e.g. silicon) [23], and by using ultra-thin substrates [24]. However, semiconductor substrates are typically required to actively control the

metamaterial response by gated structures [6] while the use of ultra-thin substrates is problematic in practical devices where integrated fluidic channels need to be incorporated, owing to their fragility and therefore low durability [25,26]. Therefore, we are motivated to find new ways to produce sensitivity enhancement using semiconductor substrates which do not employ substrate thinning.

In this work we introduce localized etching of the active area of THz SRR metamaterials, as a technique to overcome these limitations, using terahertz time-domain spectroscopy (THz-TDS) to measure the changes introduced. SRRs containing carefully designed trenches were designed to enhance their sensitivity, and the resonant frequency shifts (Δf) of the SRRs observed as a function both of etch depth, and of thickness of the overlaid dielectric material undergoing sensing. Additionally, finite element method (FEM) simulations were performed both to aid explanation and to support our experimental findings.

2. Experimental results and discussions

Figure 1(a) shows a schematic diagram of the metamaterial chips undergoing pulsed THz measurements along with the polarization direction of the incident THz waves. A linearly polarized THz pulse was generated by illuminating a bow-tie patterned, voltage-biased LT-GaAs photoconductive (PC) antenna using an 800 nm wavelength, mode-locked Ti:sapphire laser (Vitara, Coherent) which provided 20 fs pulses at an 80 MHz repetition rate. The time-resolved THz field was detected by the current generated in a similar PC antenna using a split-off portion of the same laser beam subjected to a time-delay in a retroreflector mounted on a linear translation stage. The PC THz emitter and detector each comprised a 2 μm -thick layer of LT-GaAs transferred on to a 5-mm-thick quartz substrate, fabricated using an epitaxial lift-off method [27].

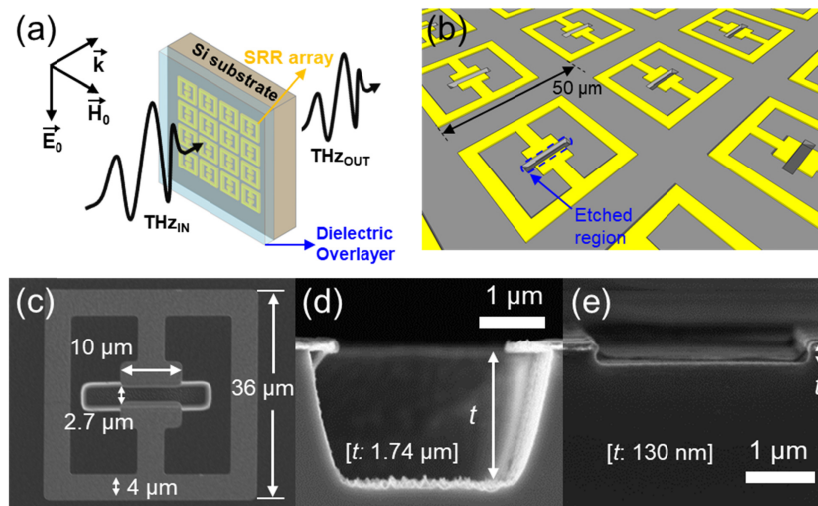


Fig. 1. (a) Schematic of THz transmission experiment for dielectric sensing using the etched metamaterials. (b) Schematic of THz metamaterials arrays with etched trenches. The periodicity of the metamaterials unit cells is indicated (c) An SEM image of the metamaterial with a trench depth of 1.74 μm . Cross-section SEM images of the metamaterials with trench depths t of (d) 1.74 μm and (e) 130 nm in the gap area.

THz pulses generated from the PC antenna were focused on to the metamaterial surface, formed on undoped silicon, with a spot size of $\sim 1.2 \text{ mm}^2$, which illuminated ~ 480 SRR elements. Pulses obtained in transmission through the array were fast Fourier transformed (FFT) and normalized with respect to reference traces obtained from transmission through an unpatterned

silicon substrate. All data was collected in a dry air environment with a humidity $< 1\%$ to remove the effect of atmospheric water absorption on the THz signal.

A schematic diagram of the metamaterial arrays incorporating the etched regions, along with the periodicity of the unit cells is shown in Fig. 1(b). Figure 1(c) shows a scanning electron microscopy (SEM) cross-sectional image of one metamaterial device prepared with a $1.74\text{-}\mu\text{m}$ -deep trench etched into the *LC* gap, which was repeated for every SRR element in the array. All metamaterial patterns were prepared using direct-write laser lithography (MLA150, Heidelberg Instruments) on a high-resistivity ($>10,000\ \Omega\text{-cm}$) undoped silicon substrate with thickness of $525 \pm 25\ \mu\text{m}$. Ti (10 nm) and Au (100 nm) metal layers deposited by electron-beam evaporation defined the THz SRR arrays, employing a metal track width of $4\ \mu\text{m}$, with outer dimensions of $36\ \mu\text{m} \times 36\ \mu\text{m}$, and a gap size of $2.7\ \mu\text{m}$. As discussed later, this choice of geometry produces a strong *LC* resonance at $\sim 0.8\ \text{THz}$ and shows sensitive response to the change of the dielectric environment as demonstrated in our previous work [21]. Reactive ion etching (RIE) was then used to form etched trenches within every *LC* gap. Positive photoresist (S1813, Shipley Inc., for trench depths $< 5\ \mu\text{m}$, and AZ9260, Micro Chemicals Corp., for trench depths $> 5\ \mu\text{m}$) was spin-coated and patterned into an etch mask, before trenches were formed using parallel-plate RIE in a gas mixture of 30 sccm SF_6 and 20 sccm O_2 at 50 W RF bias at $210\ \text{nm}/\text{min}$ etch rate. SRR arrays were fabricated with trench depths up to $7.4\ \mu\text{m}$ by adjusting the etching time. Cross-sectional SEM images of the etched metamaterials with two specimen trench depths ($1.74\ \mu\text{m}$ and $130\ \text{nm}$) in the gap area are shown as examples in Figs. 1(d) and 1(e) respectively. We note that sloped side walls were generally observed in the fabricated trench structures owing to a slight isotropy in the etching process.

To understand the effect of the etched trench structure on the effective dielectric permittivity, we performed finite element simulations using commercial software (ANSYS High Frequency Structure Simulator, HFSS). A linearly polarized incident THz plane wave and periodic boundary conditions around a single unit cell were chosen. The SRR itself was considered as a perfect sheet conductor. The silicon permittivity was taken as 11.8 ± 0.1 , which we obtained using conventional THz-TDS methods [28]. We first measured both the amplitudes and phases of the transmitted THz pulse through the silicon substrate, and calculated the permittivity of the silicon substrate using the measured phase and substrate thickness. The error of 0.1 quoted here in the silicon permittivity arises from our estimate of error in the silicon substrate thickness.

Figures 2(a) and 2(b) show the 2D electric field distribution near the gap area along the *x-y* plane (at $z = 0$) for metamaterials both without and with the etched trench structures, respectively. We note that the electric field magnitude in the gap area is significantly decreased when a trench structure with the depth of $7.4\ \mu\text{m}$ is introduced, as shown in Fig. 2(b). This is owing to a decrease in capacitance of the gap structure, which is proportional to the effective dielectric permittivity of the gap. The electric field magnitude along the *z*-axis at $x = 0$ and $y = 0$ (located at the center of the gap) is plotted in Fig. 2(c). It is clear that the decay length of the electric field magnitude below the *LC* gap, within the substrate, is larger for the metamaterials with etched gap, due to their lower effective permittivity. The simulations also reveal a small shift ($\sim 200\ \text{nm}$) in the position of the maximum electric field magnitude (inset to Fig. 2(c)) below the surface as expected when the trench structure replaces a portion of the substrate by air.

THz transmission spectra of the SRR arrays with and without the trench structure were compared to study the effects of etching (see Figs. 3(a) and 3(b) for experiment and simulation respectively). It is clear that the resonant frequency (f_0) increases as the trench structure is defined in both simulation and experiment. The Q-factor of the *LC* resonance decreased from 7.8 to 5.3 with the introduction of the trenches owing to the decrease in the capacitance. The raw data along with the zero-padded data are shown together in Fig. 3(a). The frequency resolution of $26.7\ \text{GHz}$ was obtained from the FFT of the time domain data with a temporal scan length of $37.5\ \text{ps}$, truncated before the first system reflection. In keeping with previous metamaterials

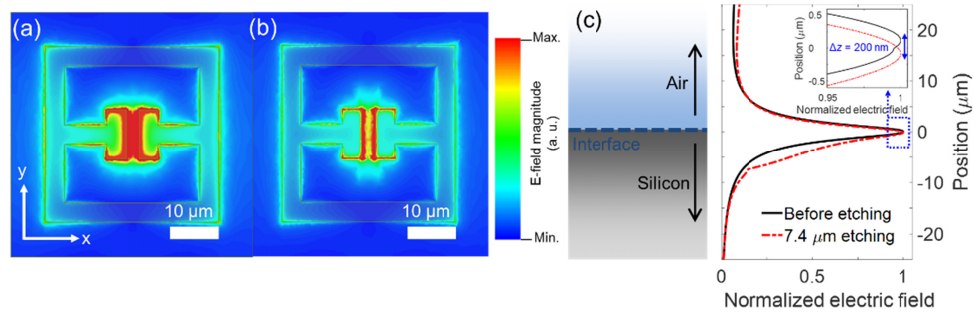


Fig. 2. Field distribution near the SRR surface (at $z = 0$) for (a) before etching and (b) after etching (c) LHS cross section showing interface between silicon and air. RHS The electric field line profile near the center of the gap structure along the z -axis before (solid black line) and after (dashed line) etching. Inset: Close-up view of the electric field line profile near the air - substrate interface highlighting the shift in the position of the maximum electric field magnitude.

studies by THz-TDS we employed zero padding both to smooth the data and to more accurately extract the position of the resonances [29,30]. To check the impact of zero padding on the assessment of peak position we employed the same procedure for each time domain data set. A numbers of zeros, n , were then progressively added to the time domain data before Fourier transform, allowing the peak position to be extracted after Fourier transform of the data. Plotting the resonant frequency of the metamaterials versus a numbers of zeros, a singular value of the resonant frequency is obtained for sufficiently large n , with a residual spread in resonant frequency which we then take as the experimental error. We note that the use of ultrathin substrates would allow longer temporal scan to be used which could overcome the need for this zero padding. In simulations, we used a trapezoidal cross-section to replicate the sloped side walls of the etch trench observed in the SEM cross-sections (Fig. 1(d)). We observed a change in resonant frequency of 116 GHz (from 788 GHz to 904 GHz) with an error of ± 0.6 GHz in the experiment and 110 GHz (from 794 GHz to 904 GHz) with an error of ± 4 GHz in the simulation after the introduction of 3.4- μm -deep trench structures. The error in the simulation results quote here arises from the experimental error in the dielectric constant of the silicon substrate, which is propagated through to the simulation. In general, the frequency of the LC resonance depends strongly on the effective dielectric permittivity in the gap area which can be expressed as a combination of the air and the substrate refractive index [21,31]. Therefore, we can significantly reduce the effective dielectric constant of the gap area by introducing the etched trenches. The shift in LC resonance induced can be expressed by $f = f_0(\varepsilon/\varepsilon_{\text{eff}})^{-\frac{1}{2}}$, where ε is the modified effective dielectric constant due to the presence of the dielectric material in the gap area, and ε_{eff} is the effective dielectric constant in the gap area before introduction of the dielectric material [16,22]. Figure 3(c) shows the resonant frequency of the etched trench metamaterials as a function of the trench depth. We found that the resonant frequency of the metamaterials increases gradually with the etching depth. The resonant frequency shift then progressively saturated for large trench depths, which occurs since the evanescent field in the gap area is highly confined near the surface (within $\sim 10 \mu\text{m}$) [20]. The deepest trench depth we could reliably obtain experimentally was $\sim 7.4 \mu\text{m}$, limited by the isotropy of the RIE etch process, which produced increasingly angled side walls shown in Fig. 1(d). Our experimental findings are in good agreement with the predictions of the simulation, although small systematic deviations (of order a few GHz, or $\sim 0.5\%$) were observed, probably owing to limitations in the spatial

resolution of the lithographic technique used during fabrication, and due to our simplification of the shape of the trench cross-section as trapezoid in the simulations.

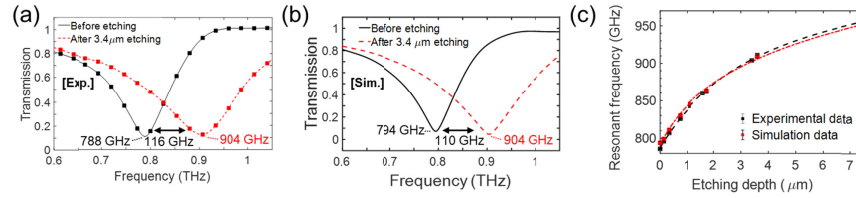


Fig. 3. (a) Experimentally obtained THz transmission of the metamaterials obtained from the raw data (dots) and zero-padded data (lines) both with (red dots and dashed line) and without (black dots and solid line) the etched trench structure with a depth of 3.4 μm (b) THz transmission of the metamaterials with (red dashed line) and without (black solid line) the etched trench structure with a depth of 3.4 μm in the FEM simulation. (c) The resonant frequency of the metamaterials as a function of trench depth in the experiment (black boxes) and simulation (red boxes). All lines are guides to the eye.

To investigate the effect of the etched trenches on device sensitivity, we fabricated THz SRR arrays with various etch trench depths, and spin-coated them with a well characterized dielectric material (Shipley S1813 photoresist) [32,33]. Figures 4(a) and 4(b) show the THz transmission of metamaterials both with and without the 3.4 μm deep trench structure, and both with and without the deposition of a 3.5 μm thick dielectric layer. We chose an etch depth of 3.4 μm since we found it was not possible to increase the dielectric film thickness systematically by spin coating when this was made any larger owing to planarity issues arising from deeper trenches. A dielectric thickness (h_{S1813}) of 3.5 μm was chosen as the sensitivity enhancement around this thickness is pertinent to the development of biosensors using THz metamaterials, since this represents a typical size for many microorganisms such as fungi, yeast and bacteria which lie the range of 1–4 μm, all of which have previously been explored with THz metamaterial sensing [1,23]. The size of the resonant frequency shift obtained by coating with a dielectric layer increased by a factor of \sim two upon etching, from 40 GHz \pm 1.2 GHz to 86 GHz \pm 1.2 GHz; simulation results were in good agreement with our experimental results as shown in Fig. 4(c). To accurately obtain the dielectric constant of S1813 for use in the simulation, we used the following relationship from our previous work, which allows us to obtain the dielectric constant without the knowledge of the film thickness once saturation conditions are reached (corresponding to film thickness $>$ 10 μm): As in previous work [34], we take $\epsilon_r = 25.06 \cdot \Delta f_{\text{sat}}/f_0 + 1$, where ϵ_r is the real part of the dielectric constant of the target materials, and Δf_{sat} is the saturated resonant frequency of the metamaterials upon deposition of thick ($>$ 15 μm) dielectric overlayers. Here, the size of the saturated resonant frequency shift (Δf_{sat}) can be described using the following relation: $\Delta f_{\text{sat}}/f_0 \approx \alpha(\epsilon_{S1813} - \epsilon_{\text{air}})/\epsilon_{\text{eff}}$, where α is the sensitivity coefficient determined by the device geometry, ϵ_{S1813} is the dielectric constant of S1813, and ϵ_{air} is the dielectric constant of air [34]. We thus obtained a dielectric constant of 2.97 for S1813 with an error of \pm 0.16 at 0.79 THz. In Fig. 4(c), we plot Δf_{sat} as a function of the trench depth with the deposition of the thick ($>$ 15 μm) S1813 overlayer for experiment and simulation. The enhancement in the resonant frequency shift was found to increase as the etch depth increases.

We confirmed that the degree of enhancement is not simply caused by an increase in the resonant frequency by comparing two SRR devices without the trenches operating at 794 GHz and 904 GHz, respectively. The resonant frequencies were adjusted by changing the LC gap distance. SRR devices operating at 904 GHz and at 794 GHz showed a saturated resonant frequency shift of 57 GHz (\pm 4 GHz) and 53 GHz (\pm 4 GHz) for deposition of thick ($>$ 15 μm) S1813 overlayers respectively. This represents an increase of \sim 4 GHz by increasing the frequency

without introducing trenches, while the experimentally determined shift introduced by the etched trenches was ~ 42 GHz (± 1.2 GHz). We also found that the resonant frequency shift for overlaid thicknesses in the main region of interest (ie for $h_{S1813} < 1 \mu\text{m}$) decreases when f_0 increases to 904 GHz. Therefore, it is almost entirely the gap introduced by the etching, rather than any change in frequency induced by etching which is responsible for the observed enhanced sensitivity. We note that ϵ_{eff} also could be reduced by replacing the substrate with a silicon-on-insulator wafer. However, the enhancement in the resonant frequency shift cannot be maximized without introducing trenches since the interaction volume between the confined electric field in the LC gap and the analyte on the metamaterial sensor surface is restricted owing to the presence of the substrate. The simulation results are in good agreement with the experimental results taking into account the size of the errors previously discussed.

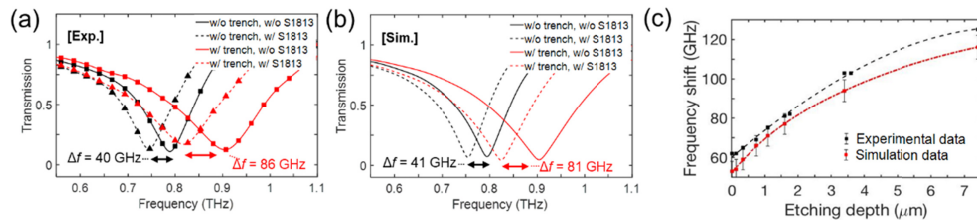


Fig. 4. (a) Experimental THz transmission of the metamaterials obtained from shown in raw data (dots) and zero-padded data (lines) both with (red dots and lines) and without (black dots and lines) the $3.4 \mu\text{m}$ depth trench structure, and both with (triangles and dashed lines) and without (square dots and solid lines) the deposition of a $3.5\text{-}\mu\text{m}$ -thick dielectric layer. (b) FEM simulation of THz transmission of the metamaterials both with (red lines) and without (black lines) the $3.4 \mu\text{m}$ depth trench structure, and both with (dashed lines) and without (solid lines) the deposition of the $3.5 \mu\text{m}$ thick dielectric layer. (c) The saturated resonant frequency of the metamaterials with the deposition of the thick dielectric overlayer ($> 15 \mu\text{m}$) as a function of the trench depth in experiment (black boxes) and simulation (red boxes). All lines are guides to the eye.

Finally, we investigated the enhancement in device sensitivity for varying thicknesses of dielectric material deposited onto the THz SRRs, both with and without the etched trenches (see Figs. 5(a) and 5(b) for experiment and simulation respectively). The resonant frequency of SRR arrays as a function of dielectric load thickness were compared under three conditions: un-etched, with a shallow trench ($0.33 \mu\text{m}$, in the linear regime of Fig. 4(c)), and with a deep trench ($3.4 \mu\text{m}$). The resonant frequency shift increases until it saturates at a specific thickness since the electric field is highly confined in the gap area. Also, the frequency shift increases as the trench depth increases owing to the decrease of the effective permittivity. From Figs. 5(a) and 5(b), the sensitivities are obtained by dividing the initial slope of the $\Delta f - h_{S1813}$ curves in the linear region ($h_{S1813} < 1 \mu\text{m}$) by the refractive index as shown in Fig. 5(c). The sensitivity of the metamaterial sensor increases from 4.3×10^{-2} GHz/nm (without the etched gap) to 11.6×10^{-2} GHz/nm (with a $3.4\text{-}\mu\text{m}$ -deep trench), which is an increase of ~ 2.7 times. We compared the sensitivity of our structure to those available in the literature by dividing the RIU sensitivity by the analyte thickness. We found the sensitivity obtained was rather higher than that obtained using ultrathin substrates (4.1×10^{-2} GHz/nm) [24], photonic crystal pillars (0.3×10^{-2} GHz/nm) [35,36], double-gap structures (1.0×10^{-2} GHz/nm) [37], a Fano resonant structure on silicon substrate (0.9×10^{-2} GHz/nm) [38] and on flexible substrate (9.0×10^{-2} GHz/nm) [39], and a toroidal resonant structure (2.4×10^{-2} GHz/nm) [40]. We also confirmed using simulations, that the sensitivity could potentially be further enhanced (\sim to 6.6 times the unetched sensitivity, data shown in Fig. 5(b)) by etching trench depths up to $30 \mu\text{m}$, which may be achieved using anisotropic etching techniques such as Inductively Coupled Plasma RIE [41]. We note that our

approach to etching the *LC* gap area can be extended to insulating substrates such as quartz [42] and sapphire [43] using this etching technique.

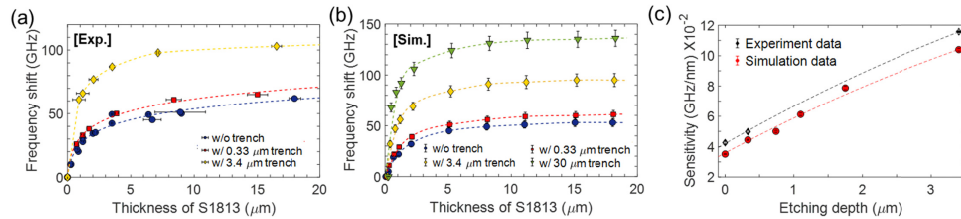


Fig. 5. Resonant frequency shift as a function of h_{S1813} for various trench depths in the range of (a) 0–3.4 μm in experiment and (b) 0–30 μm in the simulation. (c) Sensitivities extracted from the initial slopes in (a) and (b) as a function of the trench depth for un-etched, shallow etch (0.33 μm), and deep etch (3.4 μm). All lines are guides to the eye.

3. Conclusions

We have demonstrated an enhancement in sensitivity of THz metamaterials sensors to overlaid dielectric materials by the introduction of etched trenches in the *LC* gap area, which reduces the local effective dielectric permittivity. Our approach overcomes the limitations of previously reported sensitivity enhancement methods based on the use of lower-index or ultrathin substrates. In addition, our work contributes to further understanding of the operating mechanism of THz metamaterials as dielectric sensors, and could be extended to other various metamaterials-based devices such as planar metamaterials phase modulators, and metamaterials liquid sensors with integrated fluidic channels.

Funding

Engineering and Physical Sciences Research Council (EPSRC) (EP/P007449/1), (EP/P021859/1, EP/R00501X/1).

Acknowledgments

EHL acknowledges support from the Royal Society and Wolfson Foundation. Data set is online at <https://doi.org/10.5518/546>.

References

1. S. J. Park, J. T. Hong, S. J. Choi, H. S. Kim, W. K. Park, S. T. Han, J. Y. Park, S. Lee, D. S. Kim, and Y. H. Ahn, "Detection of microorganisms using terahertz metamaterials," *Sci. Rep.* **4**(1), 4988 (2015).
2. H. Tao, A. C. Strikwerda, K. Fan, C. M. Bingham, W. J. Padilla, X. Zhang, and R. D. Averitt, "Terahertz metamaterials on free-standing highly-flexible polyimide substrates," *J. Phys. D: Appl. Phys.* **41**(23), 232004 (2008).
3. H. Tao, C. M. Bingham, A. C. Strikwerda, D. Pilon, D. Shrekenhamer, N. I. Landy, K. Fan, X. Zhang, W. J. Padilla, and R. D. Averitt, "Highly flexible wide angle of incidence terahertz metamaterial absorber: Design, fabrication, and characterization," *Phys. Rev. B* **78**(24), 241103 (2008).
4. W. J. Padilla, M. T. Aronsson, C. Highstrete, M. Lee, A. J. Taylor, and R. D. Averitt, "Electrically resonant terahertz metamaterials: Theoretical and experimental investigations," *Phys. Rev. B* **75**(4), 041102 (2007).
5. W. J. Padilla, A. J. Taylor, C. Highstrete, M. Lee, and R. D. Averitt, "Dynamical electric and magnetic metamaterial response at terahertz frequencies," *Phys. Rev. Lett.* **96**(10), 107401 (2006).
6. H. T. Chen, W. J. Padilla, J. M. O. Zide, A. C. Gossard, A. J. Taylor, and R. D. Averitt, "Active terahertz metamaterial devices," *Nature* **444**(7119), 597–600 (2006).
7. S. J. M. Rao, Y. K. Srivastava, G. Kumar, and D. Roy Chowdhury, "Modulating Fundamental Resonance in Capacitive Coupled Asymmetric Terahertz Metamaterials," *Sci. Rep.* **8**(1), 16773 (2018).
8. M. Islam, S. J. M. Rao, G. Kumar, B. P. Pal, and D. Roy Chowdhury, "Role of Resonance Modes on Terahertz Metamaterials based Thin Film Sensors," *Sci. Rep.* **7**(1), 7355 (2017).

9. Z. C. Chen, N. R. Han, Z. Y. Pan, Y. D. Gong, T. C. Chong, and M. H. Hong, "Tunable resonance enhancement of multi-layer terahertz metamaterials fabricated by parallel laser micro-lens array lithography on flexible substrates," *Opt. Mater. Express* **1**(2), 151–157 (2011).
10. R. Singh, I. A. I. Al-Naib, M. Koch, and W. Zhang, "Asymmetric planar terahertz metamaterials," *Opt. Express* **18**(12), 13044–13050 (2010).
11. A. P. Tenggara, S. J. Park, H. T. Yulistira, Y. H. Ahn, and D. Byun, "Fabrication of terahertz metamaterials using electrohydrodynamic jet printing for sensitive detection of yeast," *J. Micromech. Microeng.* **27**(3), 035009 (2017).
12. S. J. Park, S. W. Jun, A. R. Kim, and Y. H. Ahn, "Terahertz metamaterial sensing on polystyrene microbeads: Shape dependence," *Opt. Mater. Express* **5**(10), 2150–2155 (2015).
13. R. Singh, A. K. Azad, J. F. O'Hara, A. J. Taylor, and W. Zhang, "Effect of metal permittivity on resonant properties of terahertz metamaterials," *Opt. Lett.* **33**(13), 1506–1508 (2008).
14. M. Liu, H. Y. Hwang, H. Tao, A. C. Strikwerda, K. Fan, G. R. Keiser, A. J. Sternbach, K. G. West, S. Kittiwatanakul, J. Lu, S. A. Wolf, F. G. Omenetto, X. Zhang, K. A. Nelson, and R. D. Averitt, "Terahertz-field-induced insulator-to-metal transition in vanadium dioxide metamaterial," *Nature* **487**(7407), 345–348 (2012).
15. H. T. Chen, J. F. O'Hara, A. K. Azad, A. J. Taylor, R. D. Averitt, D. B. Shrekenhamer, and W. J. Padilla, "Experimental demonstration of frequency-agile terahertz metamaterials," *Nat. Photonics* **2**(5), 295–298 (2008).
16. H. S. Kim, S. H. Cha, B. Roy, S. Kim, and Y. H. Ahn, "Humidity sensing using THz metamaterial with silk protein fibroin," *Opt. Express* **26**(26), 33575 (2018).
17. J. T. Hong, S. W. Jun, S. H. Cha, J. Y. Park, S. Lee, G. A. Shin, and Y. H. Ahn, "Enhanced sensitivity in THz plasmonic sensors with silver nanowires," *Sci. Rep.* **8**(1), 15536 (2018).
18. S. J. Park, S. H. Cha, G. A. Shin, and Y. H. Ahn, "Sensing viruses using terahertz nano-gap metamaterials," *Biomed. Opt. Express* **8**(8), 3551–3558 (2017).
19. L. Cong, S. Tan, R. Yahiaoui, F. Yan, W. Zhang, and R. Singh, "Experimental demonstration of ultrasensitive sensing with terahertz metamaterial absorbers: A comparison with the metasurfaces," *Appl. Phys. Lett.* **106**(3), 031107 (2015).
20. S. J. Park, S. A. N. Yoon, and Y. H. Ahn, "Effective sensing volume of terahertz metamaterial with various gap widths," *J. Opt. Soc. Korea* **20**(5), 628–632 (2016).
21. D. J. Park, S. J. Park, I. Park, and Y. H. Ahn, "Dielectric substrate effect on the metamaterial resonances in terahertz frequency range," *Curr. Appl. Phys.* **14**(4), 570–574 (2014).
22. J. F. O'Hara, R. Singh, I. Brener, E. Smirnova, J. Han, A. J. Taylor, and W. Zhang, "Thin-film sensing with planar terahertz metamaterials: Sensitivity and limitations," *Opt. Express* **16**(3), 1786–1795 (2008).
23. S. J. Park, B. H. Son, S. J. Choi, H. S. Kim, and Y. H. Ahn, "Sensitive detection of yeast using terahertz slot antennas," *Opt. Express* **22**(25), 30467–30472 (2014).
24. H. Tao, A. C. Strikwerda, M. Liu, J. P. Mondia, E. Ekmekci, K. Fan, D. L. Kaplan, W. J. Padilla, X. Zhang, R. D. Averitt, and F. G. Omenetto, "Performance enhancement of terahertz metamaterials on ultrathin substrates for sensing applications," *Appl. Phys. Lett.* **97**(26), 261909 (2010).
25. J. B. Edel, W. H. Pitchford, C. R. Crick, H.-J. Kim, A. P. Ivanov, H.-M. Kim, J.-S. Yu, T. Albrecht, K.-B. Kim, A. Pyka, J. Dziuban, and R. Puers, "Low Noise Nanopore Platforms Optimised for the Synchronised Optical and Electrical Detection of Biomolecules," *Nanofluidics* **41**, 270–300 (2016).
26. D. Lapadatu, A. Pyka, J. Dziuban, and R. Puers, "Corrugated silicon nitride membranes as suspensions in micromachined silicon accelerometers," *J. Micromech. Microeng.* **6**(1), 73–76 (1996).
27. D. R. Bacon, A. D. Burnett, M. Swithenbank, C. Russell, L. Li, C. D. Wood, J. Cunningham, E. H. Linfield, A. G. Davies, P. Dean, and J. R. Freeman, "Free-space terahertz radiation from a LT-GaAs-on-quartz large-area photoconductive emitter," *Opt. Express* **24**(23), 26986–26997 (2016).
28. Y. S. Jin, G. J. Kim, and S. G. Jeon, "Terahertz dielectric properties of polymers," *J. Korean Phys. Soc.* **49**, 513–517 (2006).
29. G. Liu, M. He, Z. Tian, J. Li, and J. Liu, "Terahertz surface plasmon sensor for distinguishing gasoline," *Appl. Opt.* **52**(23), 5695–5700 (2013).
30. W. Withayachumnankul, H. Lin, K. Serita, C. M. Shah, S. Sriram, M. Bhaskaran, M. Tonouchi, C. Fumeaux, and D. Abbott, "Sub-diffraction thin-film sensing with planar terahertz metamaterials," *Opt. Express* **20**(3), 3345–3352 (2012).
31. S. J. Park and Y. H. Ahn, "Substrate effects on terahertz metamaterial resonances for various metal thicknesses," *J. Korean Phys. Soc.* **65**(11), 1843–1847 (2014).
32. Y. Chen, I. A. I. Al-Naib, J. Gu, M. Wang, T. Ozaki, R. Morandotti, and W. Zhang, "Membrane metamaterial resonators with a sharp resonance: A comprehensive study towards practical terahertz filters and sensors," *AIP Adv.* **2**(2), 022109 (2012).
33. J. Cunningham, C. Wood, A. G. Davies, C. K. Tiang, P. Tosch, D. A. Evans, E. H. Linfield, I. C. Hunter, and M. Missous, "Multiple-frequency terahertz pulsed sensing of dielectric films," *Appl. Phys. Lett.* **88**(7), 071112 (2006).
34. S. J. Park, S. A. N. Yoon, and Y. H. Ahn, "Dielectric constant measurements of thin films and liquids using terahertz metamaterials," *RSC Adv.* **6**(73), 69381–69386 (2016).
35. F. Fan, W. H. Gu, X. H. Wang, and S. J. Chang, "Real-time quantitative terahertz microfluidic sensing based on photonic crystal pillar array," *Appl. Phys. Lett.* **102**(12), 121113 (2013).

36. F. Fan, S. Chen, X. H. Wang, P. F. Wu, and S. J. Chang, "Terahertz refractive index sensing based on photonic column array," *IEEE Photonics Technol. Lett.* **27**(5), 478–481 (2015).
37. W. Liu, F. Fan, S. Chang, J. Hou, M. Chen, X. Wang, and J. Bai, "Nanoparticles doped film sensing based on terahertz metamaterials," *Opt. Commun.* **405**, 17–21 (2017).
38. R. Singh, W. Cao, I. Al-Naib, L. Cong, W. Withayachumnankul, and W. Zhang, "Ultrasensitive terahertz sensing with high- Q Fano resonances in metasurfaces," *Appl. Phys. Lett.* **105**(17), 171101 (2014).
39. Y. K. Srivastava, L. Cong, and R. Singh, "Dual-surface flexible THz Fano metasensor," *Appl. Phys. Lett.* **111**(20), 201101 (2017).
40. M. Gupta, Y. K. Srivastava, M. Manjappa, and R. Singh, "Sensing with toroidal metamaterial," *Appl. Phys. Lett.* **110**(12), 121108 (2017).
41. F. Marty, L. Rousseau, B. Saadany, B. Mercier, O. Français, Y. Mita, and T. Bourouina, "Advanced etching of silicon based on deep reactive ion etching for silicon high aspect ratio microstructures and three-dimensional micro- and nanostructures," *Microelectron. J.* **36**(7), 673–677 (2005).
42. H. Chen and C. Fu, "An investigation into the characteristics of deep reactive ion etching of quartz using SU-8 as a mask," *J. Micromech. Microeng.* **18**(10), 105001 (2008).
43. C. M. Chang, D. Chiang, M. H. Shiao, C. T. Yang, M. J. Huang, C. T. Cheng, and W. J. Hsueh, "Dual layer photoresist complimentary lithography applied on sapphire substrate for producing submicron patterns," *Microsyst. Technol.* **19**(11), 1745–1751 (2013).